Earth Surface Processes and Landforms
Earth Surf. Process. Landforms **30**, 935–953 (2005)
Published online in Wiley InterScience (www.interscience.wiley.com). **DOI:** 10.1002/esp.1255

Using cosmogenic nuclides to contrast rates of erosion and sediment yield in a semi-arid, arroyo-dominated landscape, Rio Puerco Basin, New Mexico

Paul R. Bierman,[1]* Joanna M. Reuter,[2] Milan Pavich,[3] Allen C. Gellis,[3] Marc W. Caffee[4] and Jennifer Larsen[2]

[1] *Geology Department and School of Natural Resources, University of Vermont, Burlington, VT 05405, USA*
[2] *Geology Department, University of Vermont, Burlington, VT 05405, USA*
[3] *United States Geological Survey, National Center, Reston, VA 22092, USA*
[4] *Center for Accelerator Mass Spectrometry, Lawrence Livermore National Laboratory, Livermore, CA 94550, USA. Now at: PRIME Laboratory, Physics Department, Purdue University, West Lafayette, IN 47907, USA*

**Correspondence to:*
P. R. Bierman, Geology Department, University of Vermont, Burlington, VT 05405, USA.
E-mail: pbierman@uvm.edu

Abstract

Analysis of *in-situ*-produced ^{10}Be and ^{26}Al in 52 fluvial sediment samples shows that millennial-scale rates of erosion vary widely (7 to 366 m Ma^{-1}) through the lithologically and topographically complex Rio Puerco Basin of northern New Mexico. Using isotopic analysis of both headwater and downstream samples, we determined that the semi-arid, Rio Puerco Basin is eroding, on average, about 100 m Ma^{-1}. This rapid rate of erosion is consistent with estimates made using other techniques and is likely to result from a combination of easily eroded lithologies, sparse vegetation, and monsoon-dominated rainfall. Data from 331 stream water samples collected by the US Geological Survey between 1960 and 1995 are consistent with basin-wide, average chemical denudation rates of only about 1·4 m Ma^{-1}; thus, the erosion rates we calculate may be considered rates of sediment generation because physical weathering accounts for almost 99 per cent of mass loss.

The isotopic data reveal that sediment is generally well mixed downstream with the area-weighted average sediment generation rate for 16 headwater samples (234 ton km^{-2} a^{-1} for basin area 170 to 1169 km^2) matching well that estimated from a single sample collected far downstream (238 ton km^{-2} a^{-1}, basin area = 14 225 km^2). A series of 15 samples, collected from an arroyo wall and representing deposition through the late Holocene, indicates that ^{10}Be concentration in sediment delivered by the fluvial system has not changed appreciably over the last 1200 years despite at least two cycles of arroyo cutting and filling. Other samples (n = 21) were collected along the drainage network.

Rio Puerco erosion rates scale directly with a variety of metrics describing vegetation, precipitation, and rock erodibility. Using the headwater basins for calibration, the erosion rates for both the downstream samples and also the data set as a whole, are best modelled by considering a combination of relief and vegetation metrics, both of which co-vary with precipitation and erodibility as inferred from lithology. On average, contemporary sediment yields, determined by monitoring suspended-sediment discharge, exceed cosmogenically determined millennial-scale erosion rates by nearly a factor of two. This discrepancy, between short-term rates of sediment yield and long-term rates of erosion, suggests that more sediment is currently being exported from the basin than is being produced. Because the failure of incised channel walls and the head cutting of arroyo complexes appear to be the main sources of channel sediment today, this incongruence between rates of sediment supply and sediment yield is likely to be transitory, reflecting the current status of the arroyo cycle and perhaps the influence of current or past land-use patterns. Copyright © 2005 John Wiley & Sons, Ltd.

Received 1 September 2004;
Revised 1 April 2005;
Accepted 2 April 2005

Keywords: denudation; sediment budget; sediment transport; landscape evolution; geomorphology; land management; fluvial; cosmogenic nuclide

Introduction

The rates at which sediment is generated on hillslopes by chemical and physical weathering (sediment production or generation) and exported from drainage basins by rivers (sediment yield) can be highly variable, are poorly known, and are usually difficult to predict (Milliman and Meade, 1983; Saunders and Young, 1983). Yet, quantifying such rates over space and time is fundamental to understanding the behaviour of Earth's surface, linking surficial and deep-Earth processes (Adams, 1980; England, 1981; Pazzaglia and Brandon, 2001), and placing human impact (Hooke, 1994, 2000) in sufficient context for the development of informed land-management strategies. Semi-arid regions are of particular concern because they have some of the highest sediment yields in the world (Langbein and Schumm, 1958) and because their populations are growing rapidly (UNFPA, 2004).

Rates of sediment yield are commonly estimated using suspended sediment concentrations measured at gauging stations (e.g. Judson, 1968; Judson and Ritter, 1964). Over the past several decades, the extrapolation of such rates over longer time frames has been questioned (Kirchner *et al*., 2001; Trimble, 1977). Many contemporary land-use practices, including agriculture and the clear-cutting of forests, increase short-term sediment yields (Costa, 1975; Hewawasam *et al*., 2002; Jennings *et al*., 2003; Noren *et al*., 2002; Wolman and Schick, 1967) whereas the damming of rivers and streams usually reduces yields downstream as sediments are trapped in stilling basins (Merritts and Walter, 2003). Much of the sediment eroded from hillslopes as the result of land-use changes is not rapidly conveyed through channels; rather, it can reside on colluvial footslopes, in alluvial fans, and in river terraces for centuries or more (Schumm, 1977; Trimble, 1977; Walling, 1983).

Over the past decade, sediment generation rates, once very difficult to establish, are increasingly being estimated using measurements of cosmogenic nuclides (overwhelmingly ^{10}Be). Measurements have been made in both outcropping rock and in fluvial sediments (Bierman and Nichols, 2004; Gosse and Stone, 2001) allowing point and basin-scale areas to be evaluated, respectively. Cosmogenic nuclides, produced in the uppermost few metres of rock and soil, act as cosmic-ray dosimeters allowing calculation of near-surface residence times (Lal, 1991). Using interpretive models, such nuclide measurements can be used to estimate erosion rates, and thus rates of sediment generation if chemical weathering is considered, integrated over time frames that depend inversely on how quickly sediment is shed from the outcrop or catchment. For catchments investigated so far, integration times for cosmogenic nuclide estimates of erosion range from millennia to tens of millennia (Bierman and Nichols, 2004; Bierman *et al*., 2001). Measured basin-scale rates of erosion range from >1000 m Ma^{-1} in active mountain belts such as the Himalaya (Vance *et al*., 2003) to tens of m Ma^{-1} in cratonic settings and old mountain systems (Bierman and Caffee, 2001; Matmon *et al*., 2003b; Schaller *et al*., 2001). Comparing rates of sediment generation and sediment export (yield) tests the common assumption that the two are in steady state. Characterizing this balance (or imbalance) is an essential step in evaluating anthropogenic impacts on sediment dynamics (Brown *et al*., 1998; Hewawasam *et al*., 2003; Kirchner *et al*., 2001; Matmon *et al*., 2003a; Schaller *et al*., 2002).

In some locations, such as the southern and central Appalachians, sediment yield and erosion rate appear well-matched and thus likely in equilibrium (Matmon *et al*., 2003a,b; Reuter *et al*., 2004). In other regions, including previously glaciated regions of Europe (Schaller *et al*., 2001), parts of Idaho (Kirchner *et al*., 2001), agriculturally impacted tropical highlands (Hewawasam *et al*., 2003), and the heavily farmed mid-Atlantic Piedmont (Reuter *et al*., 2004), erosion rates and sediment yields are widely disparate. It appears that both human modification of landscapes (Hewawasam *et al*., 2003; von Blackenburg *et al*., 2004), as well as natural variability in sediment delivery (Kirchner *et al*., 2001), are responsible for these measured discordances between rates of erosion and sediment yield.

In this paper, we use a variety of data, including 52 paired analyses of *in-situ*-produced ^{10}Be and ^{26}Al measured in quartz extracted from alluvial sediment and arroyo wall samples (Table I), to better understand patterns and rates of erosion in the 16 153 km^2 drainage network of Rio Puerco Basin, northern New Mexico (Figure 1). We seek to test several hypotheses: Are rates of erosion measured cosmogenically accurate gauges of sediment generation rates? Can cosmogenic nuclides can be used to estimate erosion rates in geologically complex drainage basins with significant sediment storage? Can drainage basin characteristics (determined using geographic information system (GIS) techniques and datasets) be used to predict basin-scale rates of erosion? Are long-term rates of erosion (monitored with cosmogenic nuclides) similar to short-term rates of sediment yield (determined by suspended-sediment monitoring)?

Geological, Climatic and Geomorphic Setting

The Rio Puerco catchment is a topographically and lithologically variable arid to semi-arid area. Steep, forested headwaters with thin soils and frequent bare rock mesas are underlain by a variety of lithologies including sandstone,

Table I. Isotopic and location data for Rio Puerco sediments

Type*	Sample	Easting† (m)	Northing† (m)	Basin area (km^2)	^{10}Be measured‡ (10^5 atom g^{-1})	^{10}Be sediment generation§ (ton km^{-2} a^{-1})	^{10}Be model ε§ (m Ma^{-1})	^{26}Al Measured‡ (10^6 atom g^{-1})	^{26}Al/^{10}Be	Production factor§
	RP-01	135 329 653	3 808 956	16 153	2·90 ± 0·09	127 ± 15	49 ± 6	1·28 ± 0·07	4·4 ± 0·3	4·31
	RP-02	135 327 263	3 823 987	15 444	3·82 ± 0·11	97 ± 12	37 ± 5	1·91 ± 0·10	5·0 ± 0·3	4·36
HW	RP-03	135 327 082	3 827 397	466	7·08 ± 0·21	42 ± 5	16 ± 2	3·43 ± 0·18	4·8 ± 0·3	3·55
	RP-04	135 327 159	3 828 308	14 946	2·09 ± 0·07	179 ± 22	69 ± 8	0·96 ± 0·06	4·6 ± 0·3	4·39
	RP-05	135 315 309	3 860 236	14 225	1·58 ± 0·05	241 ± 29	93 ± 11	0·84 ± 0·05	5·3 ± 0·4	4·45
	RP-06	135 314 301	3 862 209	7 122	2·04 ± 0·07	191 ± 23	74 ± 9	1·10 ± 0·07	5·4 ± 0·4	4·57
	RP-07	135 314 680	3 862 733	7 079	1·27 ± 0·05	292 ± 35	112 ± 13	0·74 ± 0·04	5·8 ± 0·4	4·34
	RP-08A	135 286 775	3 879 635	5 107	2·69 ± 0·08	152 ± 18	58 ± 7	1·74 ± 0·10	6·5 ± 0·4	4·78
HW	RP-09	135 288 284	3 885 653	310	1·17 ± 0·07	383 ± 46	147 ± 18	0·64 ± 0·04	5·4 ± 0·5	5·22
	RP-10	135 286 280	3 882 079	4 747	3·17 ± 0·16	128 ± 16	49 ± 6	1·80 ± 0·10	5·7 ± 0·4	4·77
	RP-14	125 771 688	3 916 339	745	3·04 ± 0·09	135 ± 16	52 ± 6	1·76 ± 0·12	5·8 ± 0·4	4·81
	RP-14B	125 771 775	3 915 770	748	2·68 ± 0·08	154 ± 19	59 ± 7	1·68 ± 0·09	6·3 ± 0·4	4·81
HW	RP-18	125 753 299	3 914 283	191	24·0 ± 0·6	19 ± 2	7 ± 1	13·61 ± 0·64	5·7 ± 0·3	5·58
	RP-19	135 322 885	3 878 299	6 596	1·11 ± 0·04	341 ± 41	131 ± 16	0·61 ± 0·04	5·5 ± 0·4	4·41
HW	RP-20	135 315 120	3 911 940	303	1·18 ± 0·04	317 ± 38	122 ± 15	0·68 ± 0·04	5·7 ± 0·4	4·39
	RP-21	135 314 285	3 913 318	5 341	1·21 ± 0·06	322 ± 39	124 ± 15	0·61 ± 0·04	5·0 ± 0·4	4·57
	RP-22	135 303 526	3 938 325	4 738	1·24 ± 0·05	319 ± 38	123 ± 15	0·66 ± 0·03	5·4 ± 0·4	4·60
	RP-23	135 302 629	3 941 401	1 117	0·99 ± 0·05	420 ± 50	161 ± 19	0·51 ± 0·04	5·1 ± 0·5	4·87
	RP-24	135 320 941	3 977 229	538	0·72 ± 0·04	621 ± 74	239 ± 29	0·42 ± 0·02	5·8 ± 0·4	5·22
HW	RP-25	135 318 996	3 980 006	170	1·04 ± 0·05	389 ± 46	150 ± 18	0·57 ± 0·04	5·5 ± 0·4	4·71
HW	RP-26	135 320 250	3 980 680	358	0·49 ± 0·03	952 ± 113	366 ± 43	0·26 ± 0·02	5·2 ± 0·5	5·49
	RP-27	135 301 524	3 940 870	3 564	1·26 ± 0·05	307 ± 37	118 ± 14	0·76 ± 0·04	6·0 ± 0·4	4·52
	RP-28	135 297 164	3 946 352	1 291	0·94 ± 0·04	395 ± 47	152 ± 18	0·58 ± 0·03	6·2 ± 0·4	4·34
	RP-29	135 297 149	3 944 723	2 220	2·02 ± 0·07	196 ± 24	75 ± 9	1·18 ± 0·07	5·8 ± 0·4	4·63
	RP-30	135 296 291	3 965 004	777	0·74 ± 0·03	510 ± 61	196 ± 23	0·42 ± 0·03	5·7 ± 0·4	4·44
HW	RP-31	135 296 019	3 966 632	301	0·58 ± 0·03	661 ± 79	254 ± 30	0·36 ± 0·02	6·2 ± 0·5	4·45
HW	RP-32	135 294 902	3 966 160	471	0·87 ± 0·04	434 ± 52	167 ± 20	0·48 ± 0·03	5·5 ± 0·4	4·43
HW	RP-33	135 283 568	3 948 302	570	2·19 ± 0·08	169 ± 20	65 ± 8	1·31 ± 0·07	6·0 ± 0·4	4·34
	RP-34	135 283 510	3 948 095	1 329	2·13 ± 0·08	191 ± 23	73 ± 9	1·27 ± 0·07	5·9 ± 0·4	4·76
HW	RP-35	135 274 857	3 940 928	465	3·44 ± 0·11	130 ± 16	50 ± 6	2·03 ± 0·12	5·9 ± 0·4	5·25
HW	RP-36	135 271 613	3 939 782	207	3·75 ± 0·13	104 ± 13	40 ± 5	2·31 ± 0·14	6·2 ± 0·4	4·57
HW	RP-37	135 271 573	3 940 126	512	2·45 ± 0·09	159 ± 19	61 ± 7	1·52 ± 0·08	6·2 ± 0·4	4·56
HW	RP-38	135 297 297	3 870 915	1 169	6·40 ± 0·18	54 ± 7	21 ± 3	3·66 ± 0·20	5·7 ± 0·4	4·07
HW	RP-39	135 246 205	3 914 137	252	3·88 ± 0·14	104 ± 13	40 ± 5	2·42 ± 0·12	6·3 ± 0·4	4·72
HW	RP-40	135 246 038	3 913 862	198	5·58 ± 0·21	83 ± 10	32 ± 4	3·22 ± 0·17	5·8 ± 0·4	5·45
	RP-41	135 245 899	3 913 669	450	5·55 ± 0·23	77 ± 9	30 ± 4	3·22 ± 0·17	5·8 ± 0·4	5·04
HW	RP-42	125 768 560	3 924 962	324	1·59 ± 0·06	266 ± 32	102 ± 12	0·99 ± 0·06	6·2 ± 0·4	4·94

* HW = headwater drainage basin; no samples collected upstream.

† Location data collected using a Garmin, GPS 12, prior to the removal of selective availability so uncertainty may exceed 30 m. Data in NAD 27.

‡ Uncertainties in atomic abundances (1σ) represent quadratic addition of the error associated with the AMS ratio measurement as determined by the larger of the internal (counting statistics) and external (replication) errors, the 1σ uncertainty in Be carrier addition (2%) and Al measurement by ICP (4%). These results are corrected for ratios measured in process blanks.

§ Calculated using pixel by pixel calculation of nuclide production rate following Lal (1991) and considering only neutrons. Uncertainties in erosion and sediment generation rates are fully propagated from AMS uncertainties and include a 10 per cent 1σ uncertainty in nuclide production rates including scaling factors for altitude and latitude, as well as 5 per cent 1σ uncertainties in density, attenuation coefficients, and half-lives. Density of 2·6 g cm^{-3} assumed. Correction for altitude and latitude listed as production factor.

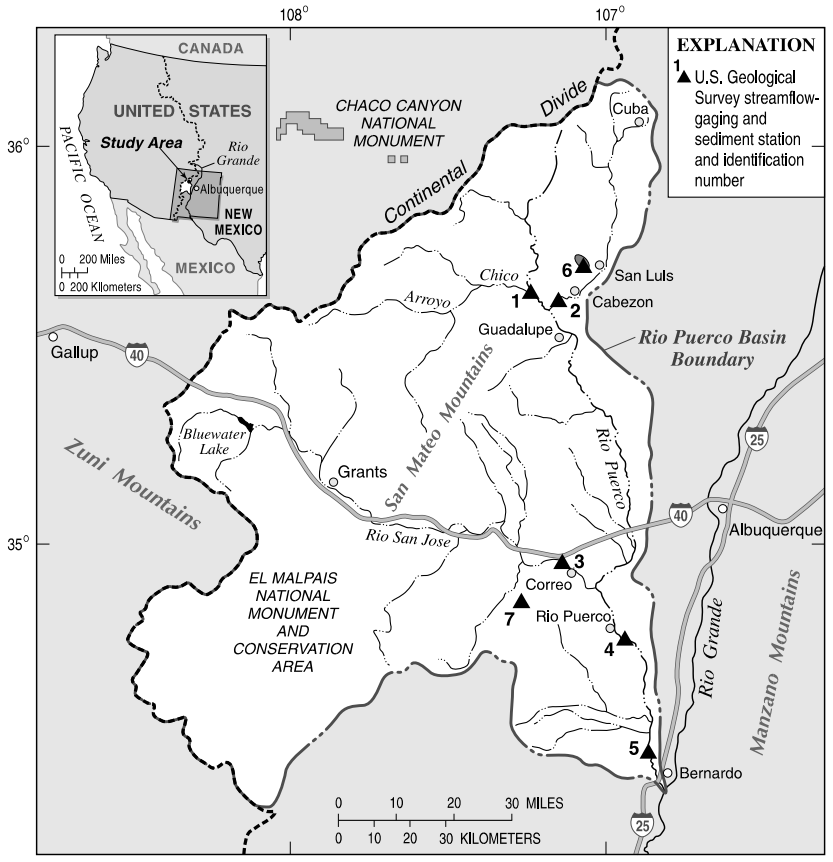

Figure 1. Location of study area. Black triangles show US Geological Survey gauging stations cited in text; numbers near stations reference Table IV. Inset shows location of Rio Puerco Basin in southwestern United States. Rio Puerco Basin is outlined and shown in white along with the drainage network. An internally drained portion of the Rio Puerco Basin in the southwest corner was not included in our sampling nor is it included in our calculations. Figure modified from Gellis *et al.* (2004).

shale, granitic, and volcanic rocks. The highlands stand in stark contrast to the grass-covered valley bottoms that are underlain by metres to tens of metres of fine-grained, unconsolidated alluvium (Figure 2). At present, much of the alluvial drainage network is deeply incised, the result of arroyo-cutting (Bryan, 1925).

Climate in the Rio Puerco Basin has changed over the timescales relevant to the isotopic analyses we report. The late Pleistocene climate of New Mexico was significantly cooler and wetter than during the Holocene or at present. The hydrologic mass balance supported large pluvial lakes in southwestern North America, including Lake Estancia to the east of the Rio Puerco Basin (Anderson *et al.*, 2002). Packrat midden data, which define palaeovegetation communities and thus climate, for New Mexico (Anderson *et al.*, 2000) indicate a significantly lower tree line. Spruce–fir forests extended into areas that are now semi-arid pinyon–juniper forest and desert scrub. This very different climate has limited influence on most of the erosion rates we obtained using ^{10}Be because in the Rio Puerco Basin measured nuclide concentrations generally indicate near-surface residence times of thousands, rather than tens of thousands of years. Only for the most slowly eroding sub-basins, where integration times exceed 10 000 years, might Pleistocene climate change influence the rates we calculate. If the conclusions of Riebe *et al.* (2001) are transferable to New Mexico from the Sierra Nevada, climate change should have little effect on erosion rate.

Climate changes over the Holocene are more germane because most ^{10}Be-inferred erosion rates for the Rio Puerco Basin integrate over millennia. The early Holocene was a period of rapid transition to a monsoon-dominated climate. Rainfall delivery from Pacific frontal systems decreased and the summer monsoon became the dominant source of precipitation (Poore *et al.*, 2005). Pluvial lakes shrank as the climate warmed and dried (Anderson *et al.*, 2002). The Holocene monsoon variability has been recently documented from correlation of packrat midden and tree-ring records from the Rio Puerco Basin with position of the Intertropical Convergence Zone (ITCZ) interpreted from Gulf of

Figure 2. Oblique aerial photograph of Rio Puerco showing channel incised into alluvium-filled basin. There is a deeply incised arroyo in the foreground and there are bedrock slopes at the basin margin. Dense riparian vegetation and steep arroyo walls indicate the lateral extent of incised channel of main stem Rio Puerco. This is sample site RP-23.

Mexico sediments (Poore *et al*., 2005). Midden data indicate that the monsoon was weak between 11 000 and 9000 ^{14}C yr BP, strong between *c*. 9000 and 4500 ^{14}C yr BP, and then weakened and became more variable since 4000 ^{14}C yr BP. Foraminifera records from the Gulf of Mexico provide independent evidence that monsoon circulation, and thus summer rainfall in New Mexico, was enhanced in the middle Holocene (*c*. 6500–4500 ^{14}C yr BP; *c*. 6980–4710 cal. yr BP). Tree-ring records from the El Malpais, in the western Rio Puerco Basin, provide more detailed information about variations in the southwest monsoon over the past 2000 years. The overall similarity between the Gulf of Mexico proxy for ITCZ position and the El Malpais records indicates century-scale variability in the southwest monsoon over the past *c*. 2000 years. Thus, the Holocene record includes both interannual and millennial-scale monsoon variability. The variability has resulted in a range of summer conditions ranging from very dry to over 500 mm of rainfall delivered by convective storms between July and October.

Although the cause of arroyo incision here and throughout southwestern North America is uncertain, arroyos have been attributed to both natural cycles and the impact of livestock grazing (Cooke and Reeves, 1976). The geomorphic and societal impacts of arroyo incision were and are dramatic (Bryan, 1925). Large volumes of unconsolidated sediment are delivered directly to the channel by a combination of geomorphic processes including scour, head cutting, and bank collapse as channels widen and deepen (Elliott *et al*., 1999). The last arroyo incision cycle began throughout the Rio Puerco Basin in the 1880s and continues in some places today. Channels were incised tens of metres below alluvial valley floors (Figure 3).

Young radiocarbon ages, and the lack of identifiable palaeosols in most arroyo walls, indicate that cutting and filling of Rio Puerco arroyos occurred repeatedly during the mid- to late-Holocene on millennial timescales (Love, 1986; Pavich *et al*., 1997) (Figure 4). Probably as a result of this cut-and-fill behaviour and the ample supply of unconsolidated alluvium, suspended-sediment concentrations in the Rio Puerco, the largest tributary of the Rio Grande, are among the highest (up to 600 000 mg l^{-1}) in the world (Gellis *et al*., 2001). Sediment concentrations in ephemeral flows of the Rio Puerco are exceeded only by those of the Yellow River in China (Milliman and Meade, 1983; Zhao *et al*., 1992). Indeed, the Rio Puerco supplies up to 70 per cent of the Rio Grande's annual sediment load (Gellis *et al*., 2004).

Methods

We collected and measured ^{10}Be and ^{26}Al in sand-sized (250 to 850 μm) alluvial sediment from 37 channel sites within the boundaries of the 20th century arroyos (Figure 5; Table I). Drainage basin areas above sample sites ranged from 170 km^2 to 16 153 km^2. Sixteen samples were collected from what we defined as headwater basins, those basins for

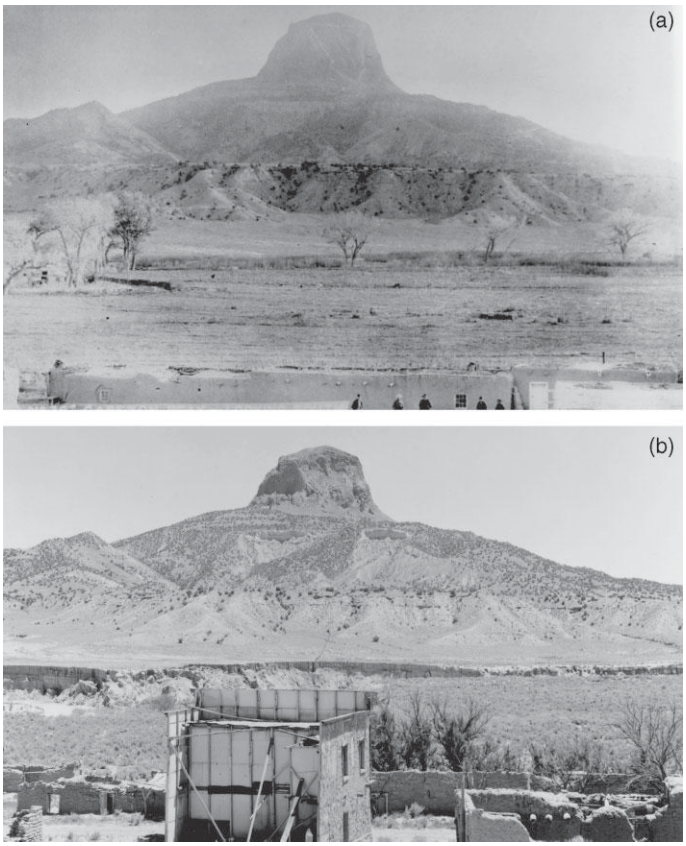

Figure 3. Paired photographs of the Rio Puerco at San Luis. (a) 1885 image showing the Rio Puerco channel before incision (photo by E.A. Bass). (b) 1977 image showing channel incised metres below the alluvial valley floor (photo by H.E. Malde). Images from USGS (2004).

Table II. Radiocarbon dates, arroyo wall exposure

CAMS no.	Depth below surface (m)	Sample name	^{14}C age (year)
81530	0·61	RP 22A 2′	685 ± 35
81532	2·56	RP 22A 8·4′	730 ± 40
81533	4·57	RP 22B 15′	635 ± 35
81534	5·79	RP 22B 19′	1235 ± 35

Age in radiocarbon years using the Libby half-life of 5568 years and measured ^{13}C values. Sample preparation backgrounds have been subtracted, based on measurements of samples of ^{14}C-free coal. Backgrounds scaled relative to sample size.

which no other samples had been collected upstream. The other 21 samples were collected farther downstream in higher-order channels. We also collected a depth profile of 15 samples and four pieces of charcoal for ^{14}C dating (Figure 5; Table II) from sediment exposed in a 6 m high arroyo wall to test for the consistency of nuclide concentration in fluvial sediment over time (near sample site RP-22).

We separated quartz from the samples and isolated ^{10}Be and ^{26}Al using standard techniques (Bierman *et al.*, 2001). Isotopic ratios were measured by accelerator mass spectrometry (AMS) at Lawrence Livermore National Laboratory (LLNL), normalized to standards prepared by Nishiizumi and cross-checked with those prepared by LLNL, and corrected using two process blanks run with each batch of six samples. Measurements of ^{26}Al and ^{10}Be in alluvial samples are extremely well correlated ($r^2 = 0{\cdot}995$, $n = 37$) so we consider primarily the more precisely measured ^{10}Be

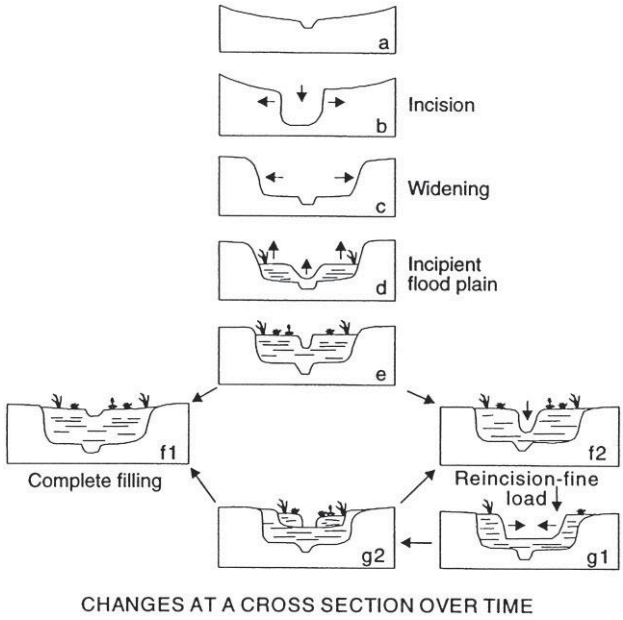

Figure 4. Idealized arroyo cycle. Initial incision of valley fill or bedrock (a) followed by deepening and widening of channel (b and c). Alluviation backfills channel cut (d and e). Subsequent incision, widening and filling may leave some sediment from prior cycles (f and g). Such cycles of cutting and filling allow us to sample sediment of different ages from arroyo walls. Figure modified from Elliott *et al.* (1999).

data for analysis of sediment generation rates. The average $^{26}Al/^{10}Be$ ratio for these samples is 5·7, similar to the production ratio of 6·0 (Nishiizumi *et al*., 1989).

To calculate rates of sediment generation from ^{10}Be and ^{26}Al measured in Rio Puerco alluvium, we used an interpretive, analytical model that relates nuclide concentration in fluvial sediment to the rate at which drainage basins are eroding and producing sediment (Bierman and Steig, 1996; Brown *et al*., 1995; Granger *et al*., 1996). To calculate effective nuclide production rates for each Rio Puerco sub-basin (Bierman and Steig, 1996), we used Lal's polynomials (Lal, 1991), with a sea-level high-latitude ^{10}Be production rate of 5·2 atoms g^{-1} quartz a^{-1} and a ^{26}Al to ^{10}Be production ratio of 6·0. The basin-wide production rate is a mean of the nuclide production rates calculated for each pixel in each basin using GIS and a 30 m digital elevation model (DEM). We accounted only for nuclide production by neutron spallation. Had we accounted for muon production (poorly parameterized and a minor component at this elevation), the erosion rates we determine would be higher at the percentage level.

In order to compare landscape-scale variability with cosmogenically calculated sediment generation rates, we used numerous publicly available data sets. Although we created and tested a variety of metrics, all can be sorted into five categories: topography, vegetation, precipitation, lithology/soil properties, and basin geometry (Table III).

The US Geological Survey (USGS) began collecting suspended sediment samples for computation of daily suspended-sediment discharge in the Rio Puerco basin in 1948 (Table IV). We computed sediment loads in the Rio Puerco following USGS procedures outlined by Porterfield (1972) and Edwards and Glysson (1988). Daily samples were collected by an observer; additional samples were collected during runoff events by USGS personnel. In 1995, automatic suspended-sediment samplers were installed at the Rio Puerco near Bernardo and the Rio Puerco above Arroyo Chico. An additional automatic sampler, which was activated at a higher river-stage level, was installed at the Rio Puerco near Bernardo in 1997. Sediment yields were determined at each station by averaging the annual suspended-sediment load and dividing by the drainage area determined by GIS analysis.

We used USGS water quality data (USGS, 2005) to estimate the average rate of chemical denudation of the Rio Puerco Basin by considering the dissolved load at the most down-stream gauging station, Bernardo (USGS 08353000, drainage area 16 153 km^2). Results are based on analyses of 331 water samples collected between 1960 and 1995 at a range of discharges (0·01 to 2720 m^3s^{-1}). Early data are measurements of mass left after total evaporation of filtered samples; later data are total post-filtration residue calculated by summing analytical determinations. Both closely match the sum of major constituents (Ca, Mg, Na, Ca, Cl, SO_4 and Si). Because regression analysis shows no trend of concentration with discharge ($r^2 = 0{\cdot}01$), we calculate loading using mean annual flow (1·18 m^3s^{-1}; 1940–2001)

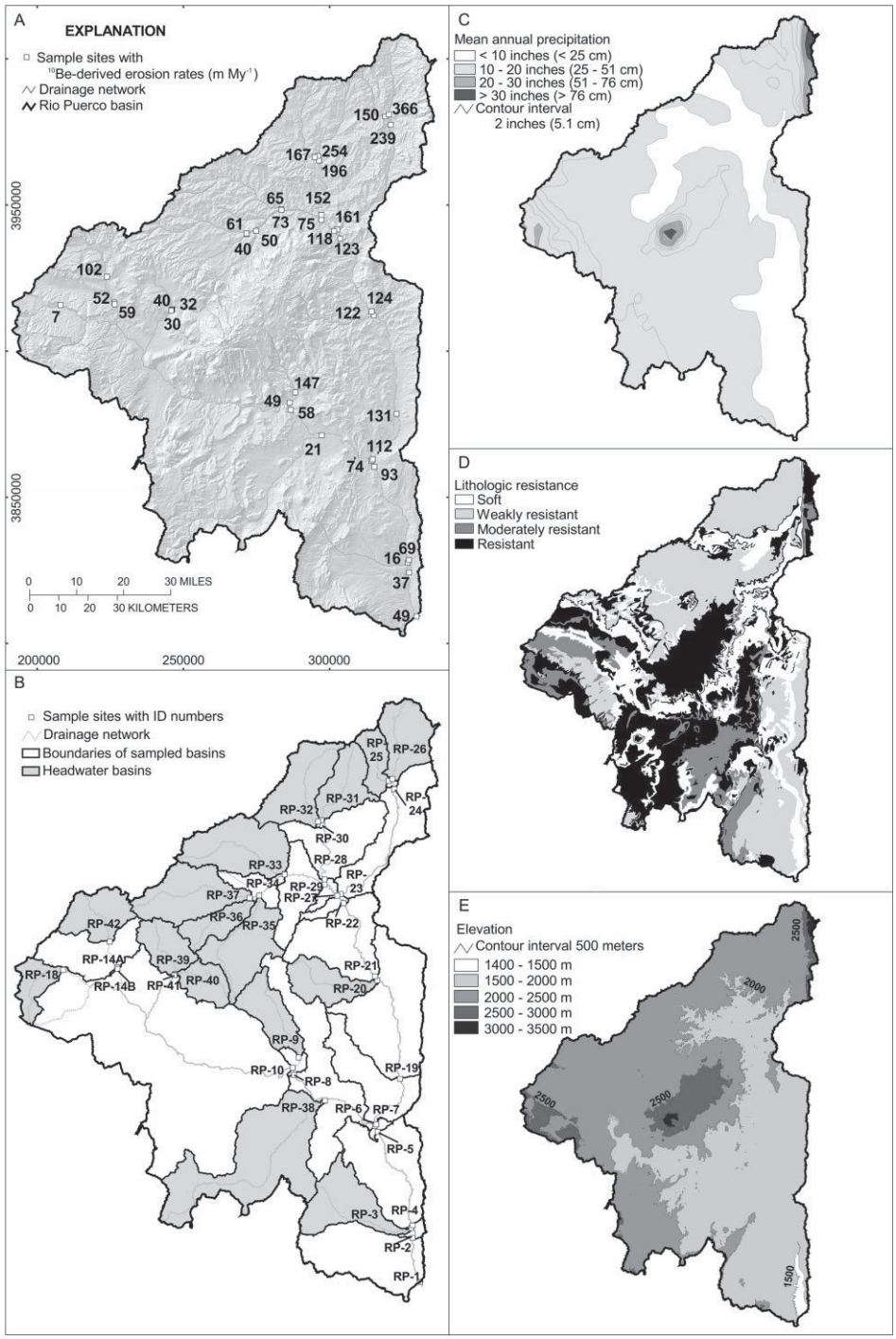

Figure 5. Maps of the Rio Puerco Basin. (A) Drainage network and locations of alluvial sediment samples collected for ^{10}Be analysis; number beside site represents basin-scale, rock-equivalent erosion rate expressed in m Ma^{-1}. Shaded relief based on digital elevation model (DEM). (B) Sample locations identified with open squares. Identification numbers are within delineated drainage basins and indicated with lines where necessary. Shaded areas are headwater basins defined by having no sample sites upstream. (C) Mean annual precipitation calculated by Oregon State University PRISM model (see Table III). (D) Resistance of rock units (J. Yount, personal communication). (E) Topography binned in 500 m intervals derived from the DEM. Coordinate System NAD83.

Table III. Landscape-scale parameters against which cosmogenically based erosion rates were compared

Category	Variable	Definition	Derived from
Basin geometry			
	DIST_US	Distance from sample site to point downstream of RP-1.	National Elevation Dataset
	AREA_KM2	Basin area.	National Elevation Dataset
Topography			
	SLP_MAX	Maximum slope within each basin.	National Elevation Dataset
	SLP_MEAN	Mean slope within each basin.	National Elevation Dataset
	SLP_STD	Standard deviation of basin slope.	National Elevation Dataset
	NEDSLPRANG	Range of slope.	National Elevation Dataset
	SLP_90TH_PERCT	90th percentile slope.	National Elevation Dataset
	ELEV_MIN	Minimum basin elevation.	National Elevation Dataset
	ELEV_MAX	Maximum basin elevation.	National Elevation Dataset
	ELEV_MEAN	Mean basin elevation.	National Elevation Dataset
	ELEVRNG	Maximum minus minimum basin elevation.	National Elevation Dataset
	ELEV_STD	Standard deviation of basin elevation.	National Elevation Dataset
	P_CURV_BW__0_1_AND_0_1	The percentage of basin area with curvature between –0·1 and 0·1.	National Elevation Dataset
	R20XNMEAN	Mean elevation minus minimum elevation in 20 km by 20 km blocks	SRTM
	R20MNMEAN	Maximum elevation minus minimum elevation in 20 km by 20 km blocks	SRTM
	R5XNMEAN	Mean elevation minus minimum elevation in 5 km by 5 km blocks	SRTM
	R5MNMEAN	Maximum elevation minus minimum elevation in 5 km by 5 km blocks	SRTM
Vegetation			
	P_52	Percentage of basin classified as 'Deserts and xeric shrublands'.	WWF Ecoregions
	P_22	Percentage of basin classified as 'Temperate coniferous forests'.	WWF Ecoregions
	P_FRST	Percentage of basin classified as 'Forested upland'.	National Land Cover Data
	P_SHRUB	Percentage of basin classified as 'Shrubland'.	National Land Cover Data
	P_HERBUP	Percentage of basin classified as 'Herbaceous upland'.	National Land Cover Data
	P_FOR_HERBUP	Percentage of basin classified as either 'Forested upland' or 'Herbaceous upland'.	National Land Cover Data
	NDVI	Calculated for 7/5/1989 image, pre-monsoon, dry year	R. Peltier, pers. comm
	TRCVMIN	Tree cover minimum value in basin.	AVHRR Continuous Fields Tree Cover
	TRCVMAX	Tree cover maximum value in basin.	AVHRR Continuous Fields Tree Cover
	TRCVRANGE	Tree cover range of values in basin.	AVHRR Continuous Fields Tree Cover
	TRCVMEAN	Tree cover mean of values in basin.	AVHRR Continuous Fields Tree Cover
Lithology and soils			
	NEW_RESIST_SCORE	Percentage soft+weak-moderate-resistant rock	J. Yount, pers. comm.
	P_VLO	Percentage very low infiltration soils	R. Peltier, pers. comm
Precipitation			
	PRSMANNMEA	Spatial mean of mean annual precipitation.	Oregon Climate Service PRISM
	PRC_AN_STD	Spatial standard deviation of mean annual precipitation.	Oregon Climate Service PRISM
	PCP_AUG_MN	Spaitial mean of mean August precipitation.	Oregon Climate Service PRISM
	PCP_AUGSTD	Spatial standard deviation of mean August precipitation.	Oregon Climate Service PRISM
	PRSMANNMIN	Value of cell in basin with lowest value of mean annual precipitation.	Oregon Climate Service PRISM
	PRSMANNMAX	Value of cell in basin with largest value of mean annual precipitation.	Oregon Climate Service PRISM
	PRSMANNRAN	Range of mean annual precipitation within basin.	Oregon Climate Service PRISM

Table IV. Summary of sediment data for the Rio Puerco Basin

Station ID or source	Station	Drainage area* (km^2)	Year sampled	Sediment yield† (ton km^{-2} a^{-1})	^{10}Be sediment generation rate (ton km^{-2} a^{-1})	^{10}Be sample	Number Figure 1
08334000	Rio Puerco above Arroyo Chico near Guadalupe	1 117	1949, 51–56, 82–98	649	408	RP23	2
08340500	Arroyo Chico near Guadalupe	2 220	1948–49, 51–56, 79–86	700	192	RP29	1
08353000	Rio Puerco near Bernardo	16 153	1948–98	242	125	RP1	4
08352500	Rio Puerco at Rio Puerco	14 946	1949–55	465	177	RP4	5
Gellis *et al.* (2004)	Arroyo Chavez	2	1996–1998	1000	224	Clapp *et al.* (2001)	6
08351500	Rio San Jose at Correo	7 122	1949–55	68	190	RP6	3

* Calculated using GIS analysis of stream network.

† Recalculated using GIS-based area calculation and yearly sediment yield information.

and the mean dissolved solid concentration determined from the 331 samples (1625 mg l^{-1}). Dissolved load was converted to lowering rate using a density of 2600 kg m^{-3}.

Data and Discussion

Cosmogenic nuclide data show that total rates of mass loss from sampled basins range from 19 to 922 ton km^{-2} a^{-1}, the equivalent of rock erosion at 7 to 366 m Ma^{-1} (ρ = 2600 kg m^{-3}). In contrast, water quality data mandate low rates of chemical weathering for the semi-arid Rio Puerco river system when considered in its entirety, the equivalent of about 1·4 m Ma^{-1}. The dominant dissolved constituent is sulphate (mean = 900 mg l^{-1}), followed by sodium (270 mg l^{-1}), calcium (180 mg l^{-1}), chloride (100 mg l^{-1}), and magnesium (41 mg l^{-1}). Beryllium-10-determined rates of erosion vary widely between sub-basins in the Rio Puerco (Table I) but in all cases they are more, usually much more, than the average value of chemical weathering. This contrast between physical and chemical rates of erosion allows us to assert that cosmogenically measured erosion rates are indeed reasonable proxies for rates of hillslope sediment generation in the Rio Puerco Basin. On average, physical erosion accounts for nearly 99 per cent of mass removal from the Rio Puerco Basin.

Erosion rates for headwater basins vary roughly with bedrock lithology. The highest rates are in the northern basin where Cretaceous to Tertiary marine shales are dominant; these are shown as weakly resistant lithologies in Figure 5D. Stratigraphically lower interbedded sandstones and shales, shown as moderately resistant lithologies in Figure 5D, have intermediate erosion rates. Basins underlain by sandstone, volcanic and plutonic rocks, shown as moderately resistant to resistant lithologies in Figure 5D, have the lowest erosion rates. An additional factor for the headwater basins is that elevation (Figure 5E) and mean annual precipitation (Figure 5C) increase in the northern part of the basin where we see the highest erosion rates on weakly resistant units. Topography and rainfall do not have similar effects at the highest elevations that are underlain by the most resistant Tertiary volcanic and Precambrian plutonic rocks. We note that the lowest measured rate (7 m Ma^{-1}) is on Quaternary volcanics in the western part of the basin.

The range in modelled rates of erosion is greater for smaller basins (<2000 km^2) than for larger basins (Figure 6). Variability appears to dampen with increasing basin area, demonstrating the importance and efficiency of sediment mixing during fluvial transport even in this semi-arid environment where flow in channels is typically ephemeral. Such mixing can be portrayed in a variety of ways, none of which are independent but all of which demonstrate different characteristics of the flow network (Figure 7). For example, when individual samples are considered by plotting them along the stream networks of which they are part, variability in nuclide concentration and thus erosion rates decreases with increasing nesting level (Figure 7A). Alternatively, considering the distance upstream from sample site RP1 (Figure 7B), the farthest downstream samples shows erosion rate variability increasing upstream as smaller headwater basins are sampled.

The basin-area average sediment generation rate (238 ton km^{-2} a^{-1}) determined from a single sample (RP-5) collected just below the confluence of the Rio Puerco's two main tributaries (drainage area = 14 230 km^2) is similar to the area-weighted average sediment generation rate (234 ton km^{-2} a^{-1}) calculated from the 16 headwater basins (average

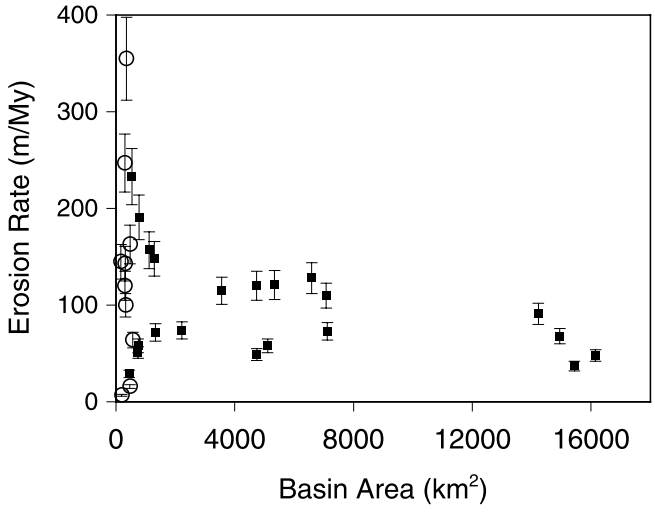

Figure 6. Basin-scale erosion rates are more variable for small basins than for larger basins demonstrating the efficacy of mixing during fluvial transport. Headwater samples are plotted as open circles. Solid squares are downstream samples. Bedrock-equivalent erosion rates calculated using density of 2600 kg m^{-3}. Error bars are 1 σ including analytical uncertainty and 10 per cent uncertainty, propagated, for nuclide production rates including scaling for elevation.

drainage area = 392 km^2) upstream of RP-5. In total, the headwater basins account for *c*. 42 per cent of the drainage area upstream of the location where sample RP-5 was collected. This finding implies that sediment is mixed well as it moves from eroding headwaters through the drainage network even in a basin of this scale. We can detect no downstream increase in nuclide concentration (Figure 6); thus, sediment is conveyed with sufficient rapidity that storage in the valley bottom, and the nuclides accumulated during such storage, do not add significantly to initial nuclide concentration generated during weathering on, and detachment from, hillslopes.

Together, the nuclide data show that uplands in the Rio Puerco Basin are lowering on average about 100 m Ma^{-1}, consistent with values determined by several other methods (Clapp *et al*., 2001; Gellis *et al*., 2001). For example, Dethier *et al*. (1988), calculated retreat rates of *c*. 100 m Ma^{-1} from hypsometric profiles of weakly lithified sandstones in the nearby Western Espanola Basin. Using sediment traps on Arroyo Chavez hillslopes, a tributary basin to the Rio Puerco, Gellis *et al*. (2004) calculated a short-term physical erosion rate of 146 ± 25 m Ma^{-1}. Beryllium-10-based erosion rate estimates are also consistent with more general, large-scale rates determined for the Colorado Plateau of 165 m Ma^{-1} and 83 m Ma^{-1} by Judson and Ritter (1964) and Holeman (1968), respectively.

Relationship between sediment yield and landscape-scale variables

The variability in nuclide concentration between samples from small basins (Figure 6) suggests that basin-to-basin differences in landscape characteristics influence erosion rates and thus nuclide concentration. Using GIS and a variety of data layers that are widely available for much of the continental United States, we investigated relationships between erosion rate and a variety of metrics related to topography, climate, vegetation, lithology and area (Figure 8; Table III).

Most characteristics we considered were not significantly related (at $p < 0{\cdot}1$) to erosion rates as modelled from ^{10}Be concentration in fluvial sediments. However, several characteristics including vegetation, climate, and erosion susceptibility appeared to be related either to ^{10}Be-determined erosion rates or the natural logs of the ^{10}Be-determind erosion rates, which we calculated in order to normalize the erosion rate distribution. Using a *p*-value cutoff $\leq 0{\cdot}1$, we find significant relationships between erosion rate and vegetation (*p_shrub*, $p = 0{\cdot}07$; *p_for_herbup*, $p = 0{\cdot}08$) as well as the variability in both annual and summer precipitation (*prc_an_std*, $p = 0{\cdot}05$; *pcp_aug_std*, $p = 0{\cdot}07$). For the natural logarithm of erosion rate, significant relationships are found for vegetation (*p_herbup*, $p = 0{\cdot}10$) and an erosion susceptibility score that considers the prevalence of soft and hard rocks (*new_resist_score*, $p = 0{\cdot}03$). None of these individual relationships is particularly strong. Pearson correlation coefficients range from 0·43 to 0·53 for the significant relationships cited above. All are positive except *p_shrub*.

Some of these relationships are consistent with what we expect to be the germane physical processes controlling sediment generation rates. For example, the inverse relationship between shrub cover and erosion might result from

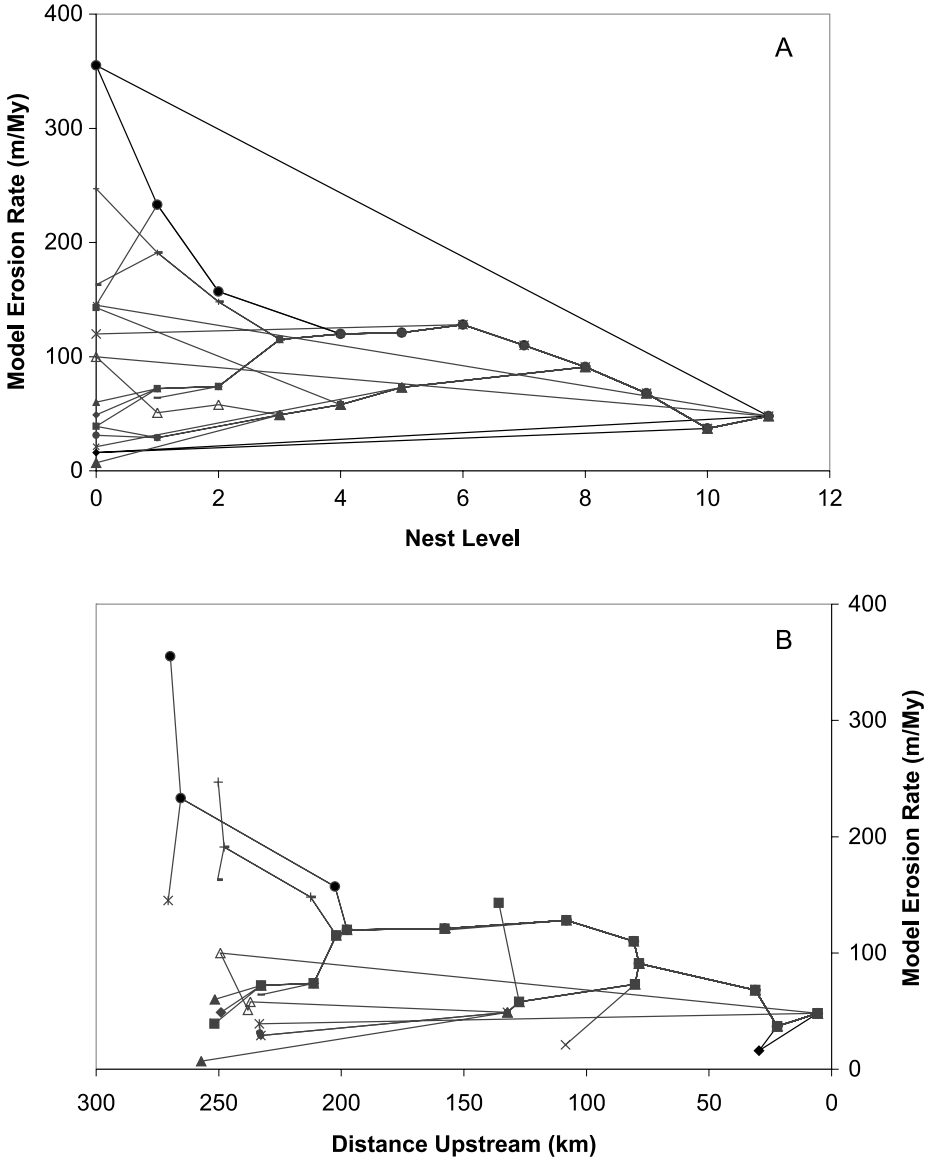

Figure 7. Erosion rates considered along stream networks. Samples connected by stream channels are plotted with similar symbols and connected with lines to indicate their interconnection in the field and the movement of sediment from one site to the next along flow paths. (A) Erosion rate variability appears to be inversely related to nesting level, where nesting level is defined as the maximum number of nested basins above the sample point; in other words, the maximum number of sample points one would pass if following the drainage to the headwaters. (B) Erosion rate variability increases along flow paths with distance upstream from RP-1, the farthest downstream sample.

the protective effect of woody vegetation. Softer rocks appear to erode more quickly. In contrast to similar work by Matmon *et al*. (2003b) in the southern Appalachians, we find no direct relationship between erosion rate and slope or elevation. Nor do we find any direct correlation of erosion rate with a variety of relief metrics, a difference from some previous findings (Ahnert, 1970; Schaller *et al*., 2001; Vance *et al*., 2003).

In order to predict the erosion rate of unsampled basins from the landscape and ^{10}Be data we do have, we used automated stepwise linear regression (SAS) to optimize an explanatory model for our data. We trained the model using only the data for the 16 headwater basins and then tested the results on both the remaining downstream samples and the data set as a whole. When we model erosion rates using multiple variables, the results are somewhat different

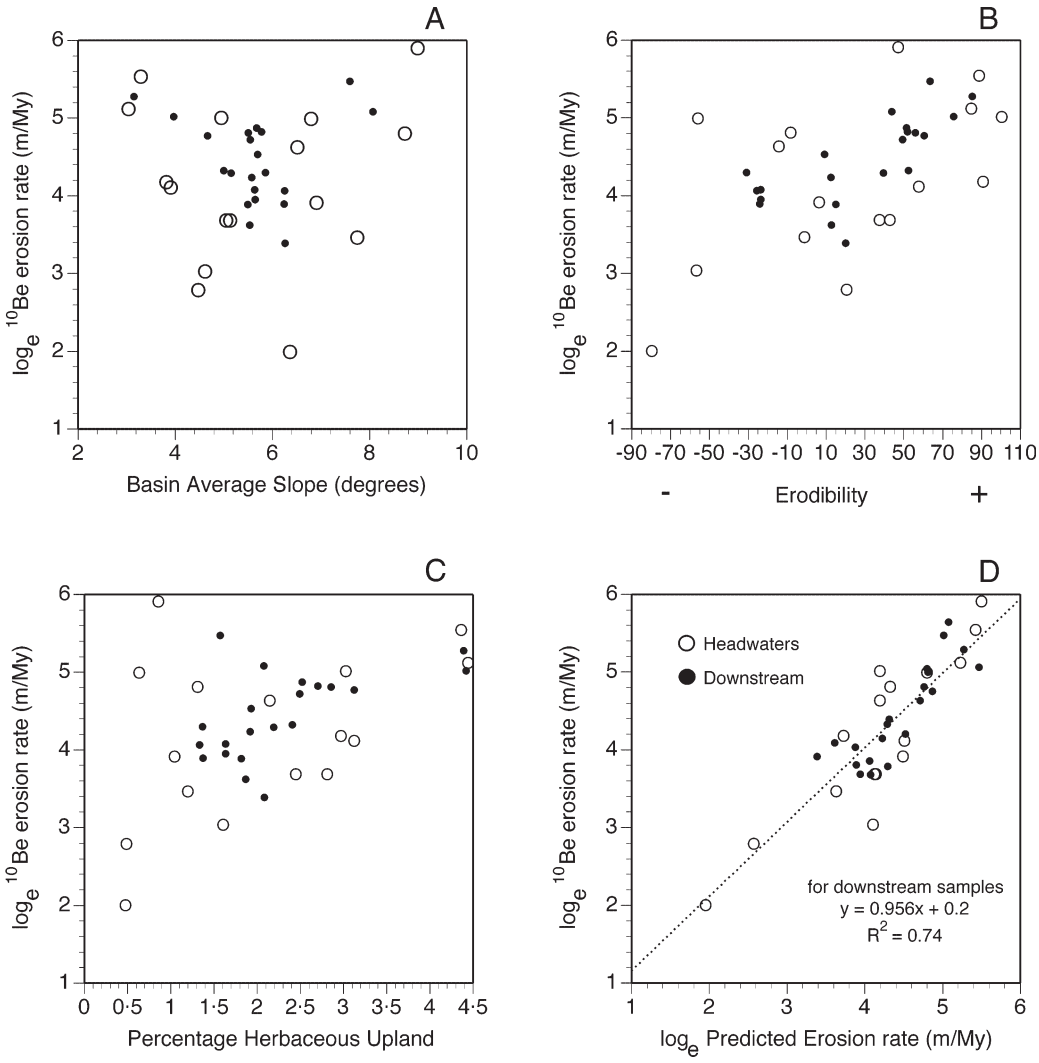

Figure 8. Scatter plots of landscape-scale variables and ^{10}Be-modelled sediment generation rates. (A) No relation between average basin slope and erosion rate. (B) Basin average erosion rate and erodibility are weakly but positively related. (C) Percentage herbaceous upland and erosion rate are weakly but positively related. (D) Regression model incorporating relief and vegetation terms explains much of the variance in erosion rates both for headwater and downstream basins (Equation 1).

from single-variable regressions. We find that erosion rates (ε, m Ma^{-1}) are best explained by a multi-variable model that considers vegetation and relief. Vegetation was important in single-variable regressions but relief was not.

The optimized model includes three variables (Table III): percentage desert and xeric shrubland (p_{52}), percentage herbaceous-covered upland (*HERB*), and relief (m) expressed as mean-minimum elevation for 400-km^2 areas (R_{20}):

$$\varepsilon = 0{\cdot}01865\ R_{20} + 0{\cdot}02175\ p_{52} + 0{\cdot}07155\ HERB_{UP} - 3{\cdot}41225 \quad (1)$$

Including these variables, the three variable model generates an r^2 value of 0·78 (adjusted $r^2 = 0{\cdot}73$) for the headwater basins ($n = 16$; $p = 0{\cdot}0003$), 0·74 for the downstream samples, and 0·77 for the data set when all 37 sediment samples are considered (Figure 8D). Inclusion of other variables in the model, such as erosion susceptibility or slope, significantly reduced goodness of fit both for the training data set and for the data set as a whole. Standardizing the variables and comparing the coefficients indicates that relief is the most important variable (1·7), percentage herbaceous covered upland is less important (1·2), and shrubland is the least important variable (0·8).

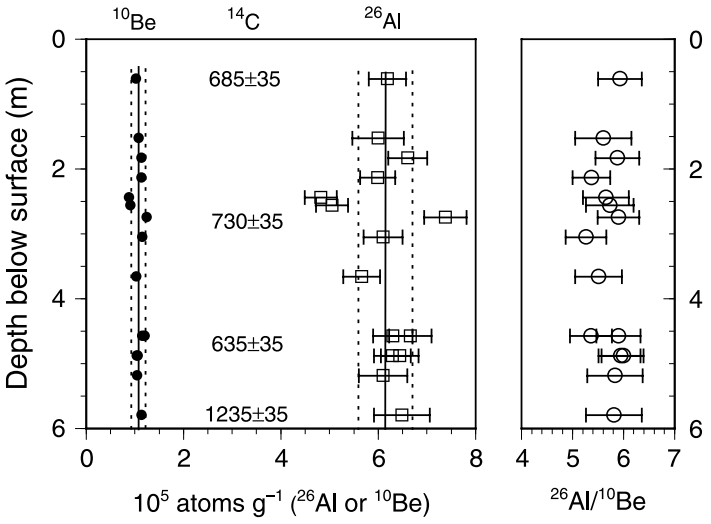

Figure 9. Concentrations of ^{10}Be and ^{26}Al and ^{26}Al/^{10}Be ratio, of 15 samples collected from arroyo wall near sample site RP-22: there is little change in nuclide concentration of deposited sediment. All error bars 1σ. Carbon-14 ages on charcoal shown at centre of graph in stratigraphic position with 1σ counting uncertainty (Table II). All but lowermost sample age are inseparable at 2σ. Solid vertical lines are mean ^{10}Be and ^{26}Al concentrations ($n = 15$ each isotope); dashed vertical lines are 1σ about the means. Three samples have nuclide concentration more than 1σ greater or less than the column average. These outliers have nuclide concentration similar to that measured in the large tributaries which join just above the sample site (RP-23, -27, -28 and -29) and most likely represent sediment contributed in spatially restricted runoff events affecting one or more, but not all, tributaries.

Many of the variables in the model are internally correlated. For example, maps of p_{52}, mean annual precipitation, and elevation look quite similar. In some places, elevation and lithology are well-correlated spatially. Because substituting these physical variables for the vegetation metrics significantly reduced model fit and predictive capability for downstream samples, we conclude that the vegetation metrics capture important, non-biotic landscape characteristics. Furthermore, the vegetation metrics are based on widely available GIS coverages and are less subjective than interpreting erosion resistance from geologic maps. In summary, it appears that no single variable or set of variables completely captures the spatial variability we measured in erosion rates.

Nuclide concentration over time

Cosmogenic nuclide concentration in sediment transported by the Rio Puerco does not appear to have changed significantly over at least the late Holocene (Figure 9). Fifteen samples from an arroyo wall exposed by channel incision in the late 19th century have similar ^{10}Be ($1{\cdot}08 \pm 0{\cdot}10 \times 10^5$ atom g^{-1}, 1σ) and ^{26}Al concentrations ($6{\cdot}14 \pm 0{\cdot}62 \times 10^5$ atom g^{-1}, 1σ). The ^{26}Al/^{10}Be ratio for these samples averages $5{\cdot}71 \pm 0{\cdot}24$ and all samples overlap at 1σ. Radiocarbon dating of the charcoal associated with the analysed sediment (Table II) indicates that the sampled arroyo wall contains sediment deposited over about the last millennium (^{14}C ages range from 635 ± 35 to 1235 ± 35 ^{14}C years). Field observations (cut-and-fill structures) and historical records suggest at least two cut cycles and one fill cycle are represented (Figure 9; Table II). The first cutting began before 1200 ^{14}C years ago and the arroyo system had backfilled by 600 ^{14}C years ago. Recent cutting began a little more than a century ago.

Beryllium-10 concentration in the arroyo wall is within the range of values measured for modern alluvium upstream and downstream of sampling site (RP-22, -23, -27 and -21; range = 0·99 to $1{\cdot}25 \times 10^5$ atom g^{-1}). Thus, when arroyo walls collapse, they deliver sediment to the channel with cosmogenic nuclide concentration indistinguishable from that of sediment in transit (cf, Clapp *et al.*, 2001). Such similarity results directly from the rapid cycle of arroyo cutting and filling that minimizes cosmic ray exposure as well as radioactive decay during storage of the thick alluvial packages. Our observation of similar ^{10}Be concentration over time, along with the buffering implied by the metre-scale depth of cosmic ray penetration (Bierman and Steig, 1996) and the *c.* 100 m Ma^{-1} erosion rate we estimate for the Rio Puerco Basin as a whole, suggest that ^{10}Be concentration measured in 20th century alluvium is representative of sediment generation rates over much, if not all, of the Holocene.

Both radiocarbon ages and the ^{10}Be analysis suggest that average sediment storage times in most Rio Puerco valley bottoms are short, on the order of no more than a few thousand years. The only exception is the lower basin, beyond the confluence of the Rio Puerco and Rio San Jose (Figure 1). Here, the alluvial valley broadens and arroyo walls give way to shallowly incised channels. Presumably channel morphology changes as more sediment is deposited from the main stem tributaries than can be carried away by the river below the junction. The inability of the lower Rio Puerco to move sediment may result from discordant flow in the two major tributaries.

The four samples collected below this major junction (RP-1, 2, 3 and 4) have lower erosion rates (higher ^{10}Be concentration) than would be predicted from the upstream samples. They also have the lowest ^{26}Al/^{10}Be ratios (4·4 to 5·0) of the sample set (Table I). Together, these observations suggest incorporation of sediment irradiated during storage in this low-gradient, downstream section of the basin. Because the exposure, burial, re-exposure and mixing history of these sediments is doubtless complex and unknowable, no unique scenario can describe the history of these grains as a group. Indeed, because each grain has a different exposure history and thus a different decay correction, interpretation of multi-grain samples such as these has always presumed that ^{10}Be behaves as a stable nuclide (Bierman and Steig, 1996).

We can make limiting calculations for burial time presuming the sediment sampled at RP-1, 2, 3 and 4 was deposited with a ^{26}Al/^{10}Be ratio ($5{\cdot}8 \pm 0{\cdot}4$) similar to the sample set as a whole (but without these four samples) and presuming the entire sample we collected was recently exhumed. If we ascribe the difference between the average ratio (5·8) and the measured ratios in RP-1, 2, 3 and 4 (4·4, 5·0, 4·8 and 4·6) we infer total burial times ranging from 300 000 to 500 000 years. This calculation neglects exposure during or after burial and any sediment recycling. Similarly, if we presume that sample RP-5 (158 000 atoms g^{-1}) is representative of main stem alluvium, then RP-1, -2 and -4 have excesses of ^{10}Be ranging from 50 000 to 220 000 atoms g^{-1}, the equivalent of 2200 to 9600 years of surface exposure at this altitude and latitude. This calculation implies significant sediment storage and reworking on much longer timescales in the lowermost Rio Puerco Basin than in the upper basin. One means to both raise the ^{10}Be concentration and the lower ^{10}Be/^{26}Al ratios in fluvial sediment would be incorporation of windblown sand; the few samples of dune sand analysed so far have high ^{10}Be contents and low ^{26}Al/^{10}Be ratios (Nishiizumi *et al.*, 1993).

Comparison of sediment generation and sediment yield rates

In five of six cases, erosion rates and thus maximum sediment generation rates in the Rio Puerco Basin are less than contemporary rates of sediment yield (Table IV). Suspended-sediment records collected at six USGS stations (*c.* 2 to 16 153 km^2) show that sediment is currently being removed from the basin faster than it is being generated (Figure 10).

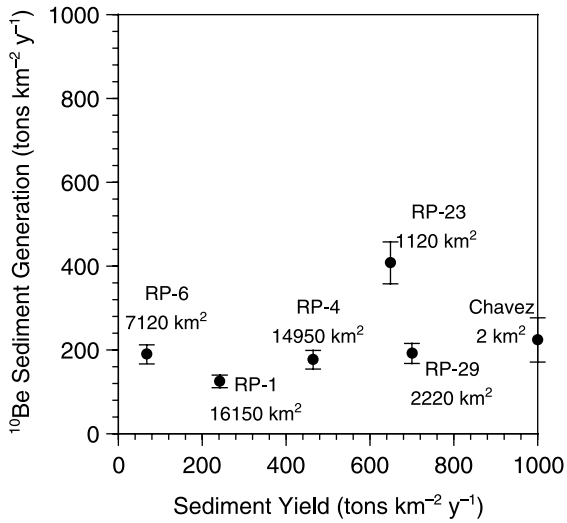

Figure 10. Suspended-sediment yield (USGS, 1948–1998; Table IV) and ^{10}Be-derived sediment generation estimates are poorly correlated ($r^2 = 0{\cdot}14$). Sediment yield exceeds sediment generation at five of the six stations where comparisons can be made. Sample number and basin area plotted next to samples. Chavez refers to previously published data for a small river system (Clapp *et al.*, 2001). Station names: RP-23, Rio Puerco above Arroyo Chico; RP-4, Rio Puerco at Puerco; RP-29, Arroyo Chico; RP-1, Rio Puerco at Bernardo; RP-6, Rio San Jose.

Such disparity is probably driven by the arroyo cycle. During periods when arroyos are incising, sediment is removed from temporary valley-bottom storage and sediment yields exceed rates of sediment generation. Conversely, during periods when arroyos are filling, sediment yield must be less than the rate of sediment generation as the volume of sediment in storage increases. The removal of sediment from valley-bottom storage and the disparity between erosion rates (^{10}Be) and sediment yield (suspended-sediment data) indicate that over human timescales the basin is not in steady state (Bryan, 1925; Cooke and Reeves, 1976). Yet, over longer timescales, the repeated cutting and filling of arroyos and the similarity of ^{10}Be concentration throughout the arroyo wall profile suggest that the nuclide activity of sediment delivered from a nearly 5000 km^2 basin has not changed over more than a millennium. This finding is consistent with effective fluvial mixing, the buffering effect of metre-scale cosmic ray penetration depths, and a lack of major changes in erosion rates over at least the Holocene.

Implications

Data presented here demonstrate that *in-situ*-produced cosmogenic nuclides have the potential to provide rapid assessment of sediment generation rates over large areas. Nuclide measurements give internally consistent data not only in small, homogeneous basins (Brown *et al*., 1995; Clapp *et al*., 2000; Granger *et al*., 1996) but also over a wide range of tributary areas, lithologies, and vegetation covers (e.g. the Rio Puerco Basin). The efficiency of fluvial mixing even by intermittent, ephemeral flows is striking (Figure 6). This mixing most likely reflects the continued addition and reworking of sediment stored for centuries to millennia in the alluvium of now-collapsing arroyo walls. On the long timescale, it appears that sediment movement in the Rio Puerco system, excepting the lowermost basin, is not transport-limited. Arroyos come and go, valley bottoms rise and fall, and although some sediment is stored for millennia, most sediment produced in the highlands is eventually exported from the basin. Indeed, Gellis *et al*. (2004) present data showing that contemporary sediment yield does not vary significantly with area over ten orders of magnitude.

Our results suggest an underlying dynamic equilibrium over the Holocene of upland sediment generation by erosion, delivery and short-term storage in valley fills, followed by repeated, episodic arroyo incision and alluvium reworking by the Rio Puerco and its tributaries. The combination of easily eroded lithologies, sparse vegetation, and monsoon-dominated rainfall (Poore *et al*., 2005) results in rapid sediment generation and efficient sediment delivery from tributaries to the main Puerco channel. Measurements of ^{10}Be in both channel sediments and from an arroyo wall section establish a background rate of landscape erosion, and thus sediment generation, that appears to have changed little over at least the late Holocene. On average, source rocks in the Rio Puerco Basin are and have been eroding through the Holocene at integrated rates of about 100 m Ma^{-1}. Most of this erosion is physical, not chemical; thus, measured rates of erosion may reasonably be considered as rates of sediment generation.

However, such an average value for erosion masks both the spatial and temporal variability of sediment delivery inherent in the Rio Puerco geomorphic system. Using GIS analysis and sample sites distributed both spatially and in basins of different character, we find that sediment generation and erosion are not spatially uniform across this landscape; rather, sediment generation rates scale with lithology, climate, vegetation, and topography. Our modelling suggests that differences in long-term erosion rates between basins may be sustained through time because metrics related to lithology, topography and thus precipitation and vegetation are important predictors of erosion even as climate and ecosystem composition change over millennia. Such differences in erosion rate over space suggest that relief may be increasing in the basin over time.

Using the ^{10}Be data, the model we have developed, and GIS-based descriptions of the landscape, it is possible to predict, albeit with significant uncertainty, the long-term sediment generation rate of any sub-basin within the Rio Puerco drainage. The model might even be applied to other nearby basins, sharing similar lithology, topography and climate. Predicting long-term erosion and thus sediment generation rates has utility for geomorphologists, hydrologists, and others interested in rates of landscape change. Such predictions may also interest land managers seeking to understand 'natural' or background sediment fluxes through fluvial systems.

Although the ^{10}Be data define the background rate of erosion well, in practice the application of such long-term, average rates to management issues is limited in this geomorphic setting. In arroyo country, sediment transport is episodic on varying timescales. Thus, even well-established average, background rates of erosion are of little use for predicting annual values of sediment yield, suspended-sediment concentration, and sediment load, which are benchmark parameters for evaluating the efficacy of land-management strategies. However, ^{10}Be-based findings can still inform land-use strategies. For example, management of slope transport systems to reduce sediment delivery to the channel, even when practical, will have little net effect on sediment yields because the ^{10}Be data and field observations suggest that much of the sediment in fluvial transport is reworked alluvium from collapsing arroyo walls and incising

gullies (Clapp *et al*., 2001). The data in this paper indicate that any regulatory framework for suspended sediment in arid and semi-arid streams and rivers needs to consider natural, time-dependent changes in sediment concentration as well as those related to human impact.

For the large basins we sampled, comparison of erosion rates (^{10}Be) with suspended-sediment yields (field monitoring) shows significant rate discrepancies (Figure 10). Average annual suspended-sediment loads routinely exceed sediment generation rates. Such a discrepancy may reflect land use and human impact through forestry and grazing (Gellis *et al*., 2004) or it may be entirely natural, the result of the arroyo cycle (Figure 4). In contrast to the difference we find, Gellis *et al*. (2004), working in a kilometer-scale basin tributary to the Rio Puerco, found that short-term (annual-scale) estimates of sediment yield on hillslopes closely matched millennial-scale cosmogenic determinations of sediment generation, except on valley floors where human disturbance is concentrated.

Erosion and incorporation of sediment from collapsing arroyo banks in sediment-mantled valley bottoms can explain both the spatial and temporal discrepancies cited above. In semi-arid, southwestern North America, arroyos cut and fill, alternately storing and releasing sediment on centennial and millennial timescales. Thus, drainage basin sediment yields are both time- and scale-dependent. When arroyos are cutting, sediment yield will exceed sediment generation. When arroyos are filling, the relationship will reverse. Such effects will only be detectable if the drainage basin is big enough to have significant alluvial fill. The areas where Gellis *et al*. (2004) found similar rates of sediment yield and erosion was generally slopes and mesa tops; there were no arroyos tapping thick, valley-bottom packages of easily erodible alluvium.

The time-dependent variability in sediment yield, and thus stream-water turbidity, suggests that contemporary suspended-sediment yields should bear little relation to long-term erosion rates (Figure 10). Suspended-sediment sampling would need to continue through an arroyo cycle to generate representative data. In contrast, sediment generation rates inferred from hillslope erosion rates can be determined by a single measurement of ^{10}Be concentration and appear to change little over time. Thus, we conclude that cosmogenic nuclides make useful monitors of long-term landscape change even in large, geomorphically complex basins with intermittent sediment storage.

Acknowledgements

We thank E. Clapp, E. Cassell and C. Massey for assistance with sample collection, and S. Nies and B. Copans for sample processing. Sample analysis supported by USGS 98HQGR1040 and NSF EAR-9396261 grants to Bierman. Comments by E. Brown, A Heimsath, an anonymous reviewer, and the 2003 University of Vermont critical writing graduate seminar greatly improved earlier versions of this paper.

References

Adams J. 1980. Contemporary uplift and erosion of the Southern Alps, New Zealand. *Geological Society of America Bulletin* **91**: 1–4.

Ahnert F. 1970. Functional relationships between denudation, relief, and uplift in large mid-latitude drainage basins. *American Journal of Science* **268**: 243–263.

Anderson RS, Betancourt JL, Mead JI, Hevly RH, Adam DP. 2000. Middle- and late-Wisconsin paleobotanic and paleoclimatic records from the southern Colorado Plateau, USA. *Palaeogeography, Palaeoclimatology, Palaeoecology* **155**: 31–57.

Anderson RY, Allen BD, Menking KM. 2002. Geomorphic expression of abrupt climate change in southwestern North America at the glacial termination. *Quaternary Research* **57**: 371–381.

Bierman P, Nichols K. 2004. Rock to sediment – Slope to sea with 10-Be – Rates of landscape change. *Annual Review of Earth and Planetary Sciences* **32**: 215–255.

Bierman PR, Caffee MW. 2001. Slow rates of rock surface erosion and sediment production across the Namib Desert and escarpment, Southern Africa. *American Journal of Science* **301**: 326–358.

Bierman PR, Steig E. 1996. Estimating rates of denudation using cosmogenic isotope abundances in sediment. *Earth Surface Processes and Landforms* **21**: 125–139.

Bierman PR, Clapp EM, Nichols KK, Gillespie AR, Caffee M. 2001. Using cosmogenic nuclide measurements in sediments to understand background rates of erosion and sediment transport. In *Landscape Erosion and Evolution Modeling*, Harmon RS, Doe WM, Kluwer: New York; 89–116.

Brown ET, Stallard RF, Larsen MC, Raisbeck GM, Yiou F. 1995. Denudation rates determined from the accumulation of in situ-produced ^{10}Be in the Luquillo Experimental Forest, Puerto Rico. *Earth and Planetary Science Letters* **129**: 193–202.

Brown ET, Stallard RF, Larsen MC, Bourles DL, Raisbeck GM, Yiou F. 1998. Determination of predevelopment denudation rates of an agricultural watershed (Cayaguas River, Puerto Rico) using in-situ-produced ^{10}Be in river-borne quartz. *Earth and Planetary Science Letters* **160**: 723–728.

Bryan K. 1925. Date of channel trenching in the arid Southwest. *Science* **62**: 338–344.

Clapp EM, Bierman PR, Schick AP, Lekach J, Enzel Y, Caffee M. 2000. Sediment yield exceeds sediment production in arid region drainage basins. *Geology* **28**: 995–998.

Clapp EM, Bierman PR, Nichols KK, Pavich M, Caffee M. 2001. Rates of sediment supply to arroyos from upland erosion determined using in situ produced cosmogenic ^{10}Be and ^{26}Al. *Quaternary Research* **55**: 235–245.

Cooke RU, Reeves RW. 1976. *Arroyos and Environmental Change in the American South-West*. Clarendon Press: Oxford.

Costa JE. 1975. Effects of agriculture on erosion and sedimentation in the Piedmont province, Maryland. *Geological Society of America Bulletin* **86**: 1281–1286.

Dethier DP, Harrington CD, Aldrich MJ. 1988. Late Cenozoic rates of erosion in the western Espanola Basin, New Mexico: Evidence from geologic dating of erosion surfaces. *Geological Society of America Bulletin* **100**: 928–937.

Edwards TK, Glysson GD. 1988. *Field methods for measurement of fluvial sediment*. US Geological Survey Open-File Report, 86–531.

Elliott JG, Gellis A, Aby S. 1999. Evolution of arroyos-incised channels of the southwestern United States. In *Incised Channels: Processes, Forms, Engineering and Management*, Simon A (ed.). John Wiley & Sons, Ltd.: Chichester; 152–185.

England P. 1981. Metamorphic pressure estimates and subsequent volumes for Alpine orogeny: an independent control on geobarometers? *Earth and Planetary Science Letters* **56**: 387–397.

Gellis AC, Pavich MJ, Ellwein A. 2001. Erosion and sediment yields in two sub basins of contrasting land use, Rio Puerco, New Mexico. *Proceedings of the 7th Federal Interagency Sedimentation Conference* V: 83–91.

Gellis AC, Pavich MJ, Bierman PR, Clapp EM, Ellevein A, Aby S. 2004. Modern sediment yield compared to geologic rates of sediment production in a semi-arid basin, New Mexico: assessing the human impact. *Earth Surface Processes and Landforms* **29**: 1359–1372.

Gosse JC, Stone O. 2001. Terrestrial cosmogenic nuclide methods passing milestones toward paleo-altimetry. *Eos, Transactions, American Geophysical Union* **82**: 6, 9, 82, 86, 89.

Granger DE, Kirchner JW, Finkel R. 1996. Spatially averaged long-term erosion rates measured from in situ-produced cosmogenic nuclides in alluvial sediments. *Journal of Geology* **104**: 249–257.

Hewawasam T, von Blackenburg F, Kubik P. 2002. Ancient landscapes in wet tropical Highlands, Sri Lanka. *Geochemica et Cosmochimica Acta* **66**: A237.

Hewawasam T, von Blackenburg F, Schaller M, Kubik P. 2003. Increase of human over natural erosion rates in tropical highlands constrained by cosmogenic nuclides. *Geology* **31**: 597–600.

Holeman JN. 1968. The sediment yield of the major rivers of the world. *Water Resources Research* **4**: 737–747.

Hooke RL. 1994. On the efficacy of humans as geomorphic agents. *GSA Today* **4**: 21724–21725.

Hooke RL. 2000. On the history of humans as geomorphic agents. *Geology* **28**: 843–846.

Jennings K, Bierman P, Southon J. 2003. Timing and style of deposition on humid-temperate fans, Vermont, United States. *Geological Society of America Bulletin* **115**: 182–199.

Judson S. 1968. Erosion of the land or what's happening to our continents. *American Scientist* **56**: 356–374.

Judson S, Ritter D. 1964. Rates of regional denudation in the United States. *Journal of Geophysical Research* **69**: 3395–3401.

Kirchner JW, Finkel RC, Riebe CS, Granger DE, Clayton JL, *et al*. 2001. Mountain erosion over 10 yr, 10 k.y., and 10 m.y. time scales. *Geology* **29**: 591–594.

Lal D. 1991. Cosmic ray labeling of erosion surfaces; in situ nuclide production rates and erosion models. *Earth and Planetary Science Letters* **104**: 424–439.

Langbein WB, Schumm SA. 1958. Yield of sediment in relation to mean annual precipitation. *EOS, American Geophysical Union Transactions* **39**: 1076–1084.

Love DW. 1986. A geological perspective of sediment storage and delivery along the Rio Puerco. In *Drainage Basin Sediment Delivery*, Hadley RF (ed.). IAHS-AISH: 305–322.

Matmon A, Bierman PR, Larsen J, Southworth S, Pavich M, Caffee M. 2003a. Temporally and spatially uniform rates of erosion in the southern Appalachian Great Smoky Mountains. *Geology* **31**: 155–158.

Matmon AS, Bierman P, Larsen J, Southworth S, Pavich M, *et al*. 2003b. Erosion of an ancient mountain range, the Great Smoky Mountains, North Carolina and Tennessee. *American Journal of Science* **303**: 817–855.

Merritts D, Walter MR. 2003. Colonial millponds of Lancaster County, Pennsylvania as a major source of sediment pollution to the Susquehanna River and Chesapeake Bay. In *Channeling Through Time: Landscape evolution, land use change, and stream restoration in the lower Susquehanna Basin, SEFOP 2003 Guidebook*, Merritts D, Walter MR, Dewitt A (eds). Franklin and Marshall College: Lancaster; 56–65.

Milliman JD, Meade RH. 1983. Worldwide delivery of river sediment to the oceans. *Journal of Geology* **91**: 1–21.

Nishiizumi K, Winterer EL, Kohl CP, Klein J, Middleton R, *et al*. 1989. Cosmic ray production rates of ^{10}Be and ^{26}Al in quartz from glacially polished rocks. *Journal of Geophysical Research, B, Solid Earth and Planets* **94**: 17907–17915.

Nishiizumi K, Kohl CP, Arnold JR, Dorn R, Klein J, *et al*. 1993. Role of in situ cosmogenic nuclides ^{10}Be and ^{26}Al in the study of diverse geomorphic processes. *Earth Surface Processes and Landforms* **18**: 407–425.

Noren AJ, Bierman PR, Steig EJ, Lini A, Southon J. 2002. Millennial-scale storminess variability in the northeastern United States during the Holocene epoch. *Nature* **419**: 821–824.

Pavich MJ, Gellis AC, Aby S. 1997. Chronostratigraphy of Quaternary alluvium, Rio Puerco basin, New Mexico. *Geological Society of America Abstracts with Program* **27**: A-372.

Pazzaglia FJ, Brandon MT. 2001. A fluvial record of long-term steady state uplift and erosion across the Cascadia Forearc High, western Washington State. *American Journal of Science* **301**: 385–431.

Poore RZ, Pavich MJ, Grissino-Mayer HD. 2005. Record of the North American Southwest Monsoon from Gulf of Mexico Sediment Cores. *Geology* **33**: 209–212.

Porterfield G. 1972. Computation of fluvial-sediment discharge: In *Geological Survey Techniques of Water-Resources Investigations of the United States Geological Survey: Book 3*. USGS: 1–66.

Reuter JM, Bierman PR, Pavich M, Gellis A, Larsen J. 2004. *Erosion of the Susquehanna River Basin: Assessing relations between 10-Be derived erosion rates and basin characteristics*. Presented at Northeastern Section (39th Annual) and Southeastern section (53rd Annual) Joint Meeting, Tysons Corner, Virginia, paper 35-3.

Riebe CS, Kirchner JW, Granger DE, Finkel RC. 2001. Minimal climatic control on erosion rates in the Sierra Nevada, California. *Geology* **29**: 447–450.

Saunders I, Young A. 1983. Rates of surface processes on slopes, slope retreat, and denudation. *Earth Surface Processes and Landforms* **8**: 473–501.

Schaller M, von Blanckenburg F, Hovius N, Kubik PW. 2001. Large-scale erosion rates from In situ-produced cosmogenic nuclides in European river sediments. *Earth and Planetary Science Letters* **188**: 441–458.

Schaller M, von Blanckenburg F, Veldkamp A, Tebbens LA, Hovius N, Kubik PW. 2002. A 30 000 yr record of erosion rates from cosmogenic 10Be in Middle European river terraces. *Earth and Planetary Science Letters* **204**: 307–320.

Schumm SA. 1977. *The Fluvial System*. Wiley: New York.

Trimble SW. 1977. The fallacy of stream equilibrium in contemporary denudation studies. *American Journal of Science* **277**: 876–887.

UNFPA. 2004. Annual Report 2001. http://www.unfpa.org/about/report/2001/index.htm [23 August 2004].

USGS. 1948–1998. http:climchange.cr.usgs.gov/rio_puerco/erosion/streamflow.html

USGS. 2004. USGS Rio Puerco Online. http://climchange.cr.usgs.gov/rio_puerco/archive/bass.html [28 July 2004].

USGS. 2005. US Geological Survey water quality data. http://nwis.waterdata.usgs.gov/nwis/ [February 2005].

Vance D, Bickle M, Ivy-Ochs S, Kubik PW. 2003. Erosion and exhumation in the Himalaya from cosmogenic isotope inventories of river sediments. *Earth and Planetary Science Letters* **206**: 273–288.

von Blanckenburg F, Hewawasam T, Kubik PW. 2004. Cosmogenic nuclide evidence for low weathering and denudation in the wet, tropical highlands of Sri Lanka. *Journal of Geophysical Research* **109**: 1–22.

Walling DE. 1983. The sediment delivery problem. *Journal of Hydrology* **65**: 209–237.

Wolman MG, Schick AP. 1967. Effects of construction on fluvial sediment, urban and suburban areas of Maryland. *Water Resources Research* **3**: 451–464.

Zhao W, Jiao E, Wang M, Meng X. 1992. Analysis of the variation of sediment yield in Sanchuanhe River Basin in the 1980s. *International Journal of Sediment Research* **7**: 1–20.

